

## LETTERS

# Meteoritic dust from the atmospheric disintegration of a large meteoroid

Andrew R. Klekociuk<sup>1</sup>, Peter G. Brown<sup>2</sup>, Dee W. Pack<sup>3</sup>, Douglas O. ReVelle<sup>4</sup>, W. N. Edwards<sup>2</sup>, Richard E. Spalding<sup>5</sup>, Edward Tagliaferri<sup>3</sup>, Bernard B. Yoo<sup>3</sup> & Joseph Zagari<sup>1</sup>

Much of the mass of most meteoroids entering the Earth's atmosphere is consumed in the process of ablation. Larger meteoroids (>10 cm), which in some cases reach the ground as meteorites, typically have survival fractions near 1–25 per cent of their initial mass<sup>1</sup>. The fate of the remaining ablated material is unclear, but theory suggests that much of it should recondense through coagulation as nanometre-sized particles<sup>2</sup>. No direct measurements of such meteoric 'smoke' have hitherto been made<sup>3</sup>. Here we report the disintegration of one of the largest meteoroids to have entered the Earth's atmosphere during the past decade, and show that the dominant contribution to the mass of the residual atmospheric aerosol was in the form of micrometre-sized particles. This result is contrary to the usual view that most of the material in large meteoroids is efficiently converted to particles of much smaller size through ablation<sup>4</sup>. Assuming that our observations are of a typical event, we suggest that large meteoroids provide the dominant source of micrometre-sized meteoritic dust at the Earth's surface over long timescales.

United States Department of Defense space-based infrared sensors detected a large meteor in flight at an altitude of approximately 75 km at 12:07:20.975 UT (universal time) on 3 September 2004 at latitude 67.72° S, longitude 16.89° E. Space-based Department of Energy (DoE) visible light sensors also detected the fireball (Fig. 1). Subsequently, the emissive debris trail from the fireball was measured, extending from 56–18 km altitude and remained detectable at infrared wavelengths owing to solar scattering for over an hour. Two distinct disintegration features were visible along the path, at 32 km and 25 km altitude. We hereafter refer to this fragmentation region as 'ground zero'. Application of entry modelling<sup>5,6</sup> of the light curve and trajectory data yielded initial mass estimates between  $(0.6\text{--}1.9) \times 10^6$  kg, depending on the choice of various parameters in these models. Extrapolating a previously determined relation between optical energy and total energy<sup>7</sup> derived for smaller bolides yields an estimate for total initial energy of  $(5.4 \pm 0.4) \times 10^{13}$  J (equivalent to  $13 \pm 1$  kilotons of exploding TNT) corresponding to a mass of  $(0.65 \pm 0.05) \times 10^6$  kg. The original solar orbit of the body (Supplementary Table 1) is similar to near-Earth asteroids of the Aten group.

In addition to the satellite energy estimates, five infrasound stations detected acoustic gravity waves from the fireball, with the furthest detection being 13,000 km from ground zero. Using a recent calibration between wind-corrected observed fireball acoustic amplitudes and satellite yields<sup>8</sup>, a mean source energy of  $(1.2 \pm 0.3) \times 10^{14}$  J ( $28 \pm 6$  kilotons of TNT) was obtained from signals detected at the four closest stations, equivalent to a mass of  $(1.4 \pm 0.3) \times 10^6$  kg. The range of initial mass estimates from modelling and the optical and acoustic data correspond to a body

of diameter 7–10 m, assuming a mass density typical of chondritic meteorites<sup>9</sup> of  $\rho = 3,500 \text{ kg m}^{-3}$ .

Some 7.5 h after the satellite observation, an anomalous 'cloud' was detected in the upper stratosphere by a polarization Rayleigh light detection and ranging (lidar) instrument at Davis station (68.6° S, 78.0° E) in Antarctica<sup>10</sup> (Fig. 2). The cloud, which was directly related to the fireball event (as discussed below), was situated above the maximum height at which polar stratospheric clouds have previously been detected in September at Davis (~20 km altitude) and other similar-latitude sites<sup>11,12</sup>. As determined by the lidar, local radiosondes and the Atmospheric Infrared Sounder (AIRS) satellite instrument<sup>13</sup>, temperatures in the vicinity of the cloud were near 240 K. This was ~55 K warmer than the expected frost-point for nitric acid trihydrate, which has the highest equilibrium temperature of solid polar stratospheric cloud constituents.

Using the location and time of the fireball, we examined three air parcel trajectory models to investigate aerosol dispersal in the context of the lidar observations. According to the best-fit model (from the Goddard Spaceflight Center<sup>14</sup>), air parcels from 32 km altitude at ground zero passed directly over Davis at 28.5 km altitude near 19:50 UT. This closely agrees with the onset of the strongest lidar backscatter shown in Fig. 2. Air from below 30 km altitude at ground

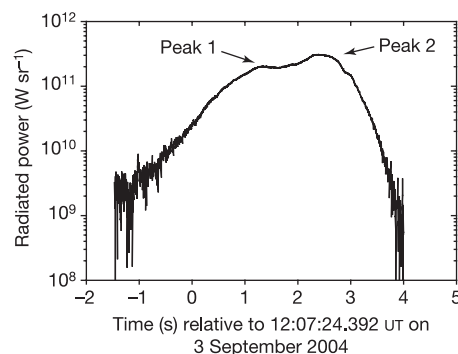


**Figure 1 | Optical light curve for the 03 Sep 2004 fireball as measured by DoE space-based sensors.** The signal was approximately 5.5 s in duration and exhibited two peaks due to discrete fragmentation events. These are assumed to be correlated with the features along the infrared track at altitude 32 km (located at 67.68° S, 18.00° E) and at 25 km altitude (67.67° S, 18.17° E). Intersection of the projected path with the Earth was at 67.64° S, 18.83° E (WGS-84 ellipsoid). The maximum radiated power of the event was  $3.08 \times 10^{11} \text{ W sr}^{-1}$ , and the total radiated energy was  $7.26 \times 10^{12} \text{ J}$  (assuming that the fireball radiated as a 6,000-K blackbody). At its brightest, the bolide had an absolute visual magnitude of  $M_v = -24$ .

<sup>1</sup>Space and Atmospheric Sciences, Australian Antarctic Division, Kingston, Tasmania 7050, Australia. <sup>2</sup>Department of Physics and Astronomy, University of Western Ontario, London, Ontario N6A 3K7, Canada. <sup>3</sup>The Aerospace Corporation, 2350 E. El Segundo Blvd, El Segundo, California 90245-4691, USA. <sup>4</sup>Los Alamos National Laboratory, PO Box 16663, MS J577, Los Alamos, New Mexico 87545, USA. <sup>5</sup>Sandia National Laboratory, Org. 5740, MS 0973, PO Box 5800, Albuquerque, New Mexico 87185, USA.

zero was modelled as passing more than 100 km north of Davis, and this suggests that the debris observed by lidar is from the upper infrared fragmentation event, but not the lower event. Based on the observed durations of the cloud features and using inferred wind fields, we estimate that the lower limit on the zonal extent of the trail at a given altitude was  $\sim 75$  km as it passed Davis.

We modelled the arrival time–altitude profile of sedimenting particles at Davis (Fig. 3) to examine the potential range of particle sizes<sup>15</sup>. The main front of the lidar cloud features is well represented by the arrival of particles with radii of  $\sim 5$   $\mu\text{m}$  or less. In addition to the features shown in Fig. 2, narrow (and weak) aerosol layers with a mean backscatter ratio of  $\sim 0.05$  above their immediate background, and that were tilted in the arrival time–altitude plane, were observed by lidar at lower altitudes. As indicated in Fig. 3, the upper layer had behaviour consistent with the sedimentation of particles with radii of  $\sim 10$ – $20$   $\mu\text{m}$  originating near 30 km altitude at ground zero. The lower layer appears to represent the leading edge of an ensemble of different plumes of large particles.

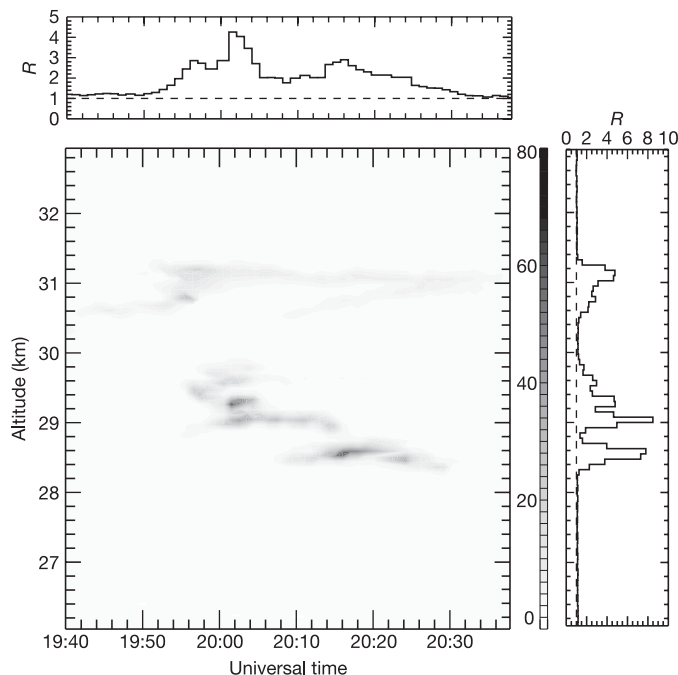


**Figure 2 | The first unambiguous detection of lidar backscatter from the dust trail of a large meteoroid.** Plotted is the lidar-derived total backscatter ratio  $R$  at a wavelength of 532 nm for a segment of the Davis observations on 3 September 2004, showing discrete structures detected between 19:38 UT and 20:37 UT. Here  $R = 1 + \beta_m/\beta_a$ , where  $\beta_m$  and  $\beta_a$  are the sums of the molecular and aerosol backscatter coefficients for orthogonally polarized signal components, respectively. The lidar retrieval was calibrated using the molecular number density inferred from AIRS satellite data<sup>13</sup>. Also shown are mean vertical and horizontal cross-sections for  $R$ . To investigate the time–altitude profile of aerosols detected by the lidar, three models of atmospheric transport were considered: the Goddard Spaceflight Center (GSFC) model<sup>14</sup>, the Hybrid Single-Particle Lagrangian Integrated Trajectory (HYSPLIT) model from the National Oceanic and Atmospheric Administration, and the British Atmospheric Data Centre Trajectory Service. Of these models, only HYSPLIT evaluated particle sedimentation. All of the models clearly showed that for altitudes near 32 km, ground zero was directly upwind of Davis, with a strong (up to  $\sim 95$   $\text{m s}^{-1}$ ) dominantly zonal flow linking the two sites. The speed of the flow accounted for the time difference between the bolide and lidar detections to better than 7%. In addition, the models suggested that the main cloud features represented suspended or weakly sedimenting particles (that is, descending by less than a few kilometres per day). The best agreement with the observations was obtained with the GSFC model using GSFC Data Assimilation Office (DAO) meteorological fields and diabatic corrections.

The lidar depolarization ratio<sup>16</sup> as a function of backscatter ratio (Fig. 4) shows that the clouds were dominated by non-spherical (solid) aerosols. The lidar data also show that these aerosols were optically thin. We could only place an upper limit of  $0.01 \text{ km}^{-1}$  on the mean aerosol optical depth over the altitude range 28–31.5 km. This property was used together with the observed frequency distributions of depolarization ratio and backscatter ratio (in particular, the clustering into two groups shown in Fig. 4) to constrain the parameter space of effective particle radius, number density, shape and composition. This was done through comparison with scattering calculations<sup>17,18</sup> for randomly oriented irregular spheroids comprising six cosmic dust analogue materials<sup>19–21</sup> for particle radii up to 5  $\mu\text{m}$ ; meteoric aerosol, glassy olivine, glassy pyroxene, silicon, iron and iron oxide. We found that the simplest match to the observed range and distribution of depolarization ratios was exhibited by olivine and pyroxene (materials found in chondritic meteorites<sup>20</sup>) for effective radii of between  $\sim 0.3$  and  $\sim 1.1$   $\mu\text{m}$  and nearly spherical shapes (shape factors between 0.9 and 1.1).

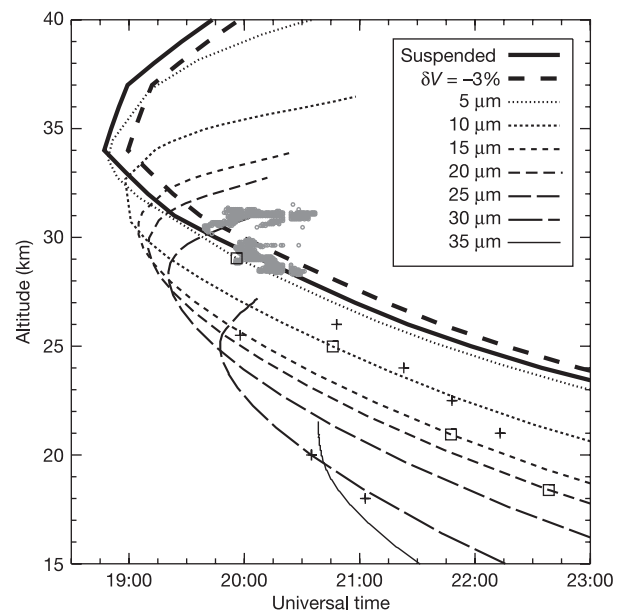


**Figure 3 | Comparison between the time–altitude characteristics of the lidar-detected aerosols and the predictions of a sedimentation model.** The model evaluated trajectories for spherical particles along the lagrangian path between ground zero and Davis using interpolated United Kingdom Meteorological Office (UKMO) Stratospheric Assimilated Data<sup>15</sup>. The plotted lines show the arrival time–altitude loci obtained from the model for the longitude of Davis, assuming a particle mass density of  $3,500 \text{ kg m}^{-3}$ . Overlaid are lidar scattering features (grey) having  $R > 2$  (see Fig. 2). The crosses refer to weak aerosol features described in the text. Open squares show where particles of different radii released from ground zero at 30 km altitude would lie. The bold dashed line shows the case of suspended particles for a wind speed 3% lower than its mean value, to indicate one side of the expected spread in arrival times due to the influence of atmospheric gravity waves. The UKMO wind speed reached a peak value of  $\sim 95 \text{ m s}^{-1}$  near 34 km altitude. The vertical gradient in the wind speed below the peak was  $4 \text{ m s}^{-1} \text{ km}^{-1}$  and this accounted for the majority of the arrival time–altitude dispersion of the leading cloud fronts evident in Fig. 2. The cloud features above  $\sim 30$  km appear more complex and extended than those at lower altitudes, and this may be related to shearing in the wind profile near 34 km, or produced by the fireball itself. An additional possibility is that the upper layers represent relatively heavy particles from higher altitudes (35 km to at least 60 km, the top of the UKMO model) that had fallen to this region. However, this association is problematic because the size distribution of the particles would need to be extremely narrow because of the small vertical extent of this cloud layer as a function of time.

Olivine gave the best agreement between the limiting depolarization values  $\delta_1$  for the two aerosol associations (Groups 1 and 2, shown in Fig. 4) and peaks in the calculated depolarization at effective radii  $r$  of  $0.41 \pm 0.12$  and  $0.98 \pm 0.29 \mu\text{m}$ , respectively. Using lidar-derived mean backscatter coefficients and theoretical backscatter cross-sections we estimated effective particle-number densities  $N$  for the two groups as  $(6.0 \pm 2.7) \times 10^6 \text{ m}^{-3}$  (Group 1) and  $(1.7 \pm 0.4) \times 10^6 \text{ m}^{-3}$  (Group 2).

Taking the values of  $N$ , together with  $r$  and mass density  $\rho$ , and the inferred dimensions of the lidar-detected cloud (zonal  $\sim 75$  km, meridional  $\sim 200$  km from trajectory modelling, vertical  $\sim 3$  km from Fig. 2), we estimate the total mass of the aerosols as  $(1.1 \pm 0.3) \times 10^6$  kg. This value compares favourably with the meteoroid mass from the satellite and airwave data given above. We note that this mass estimate probably relates only to part of the debris cloud (that is, the upper fragmentation event) and hence is a lower limit. Further trajectory and scattering modelling is required to refine these values. We also note that iron and iron oxide gave reasonable depolarization values at radii less than  $\sim 0.3 \mu\text{m}$  for highly

non-spherical particle shapes. However, the inferred optical depth for these aerosols was significantly larger than that deduced from the lidar observations.

Our measurements suggest that a substantial fraction of the total ablated mass from large (metre-sized) chondritic bodies entering the atmosphere is deposited as  $\sim$ micrometre-sized dust. This dust is likely to have atmospheric residence times of weeks to months. Micrometre-sized aerosols play a crucial role in climate forcing, through direct (radiative) and indirect (cloud nucleation) effects, as well as in ozone depletion through heterogeneous reactions. Aerosols with radii between about  $0.05 \mu\text{m}$  and  $1 \mu\text{m}$  scatter the most light per unit mass, and tend to have the longest atmospheric residence times<sup>22</sup>. The conventional view is that the background meteoritic aerosol flux is of low significance in climate forcing primarily because nanometre-sized particles dominate the size spectrum<sup>23</sup>. In light of our findings, this view requires further investigation.

If most of the mass from large ( $>0.1$  m) meteoroid disintegrations is reduced to micrometre-sized particles, this process would dominate the influx to the Earth's surface of extraterrestrial dust at these sizes. Indeed, the mass flux from primary meteoroids of  $1 \mu\text{m}$  and smaller is a few hundred tonnes per year, which is less than the mass delivered by sizes  $>0.1$  m on century timescales<sup>24</sup>. Although our measurements apply strictly to larger meteoroids disintegrating lower in the atmosphere (constituting a mass influx of  $\sim 1$  kt per year), a substantial fraction of the total ablated mass of smaller meteoroids may also be partitioned into larger (micrometre versus nanometre) meteoric dust. Micrometre-sized ablation products cannot easily be measured individually in large numbers at the Earth's surface and so the mass distribution of meteoric material at such small sizes is largely unknown<sup>25</sup>. In particular, models of atmospheric heating of interplanetary dust generally treat meteoroids as single ablating bodies, whereas much evidence suggests<sup>26</sup> that small ( $10^{-8}$  kg) meteoroids near the peak of the mass influx curve ablate as a collection of grains (dustballs), emphasizing the importance of fragmentation. In such a situation, the survival of a large fraction of the total incident meteoroid mass as micrometre-sized particles to the Earth's surface would be possible.

Received 16 March; accepted 1 June 2005.

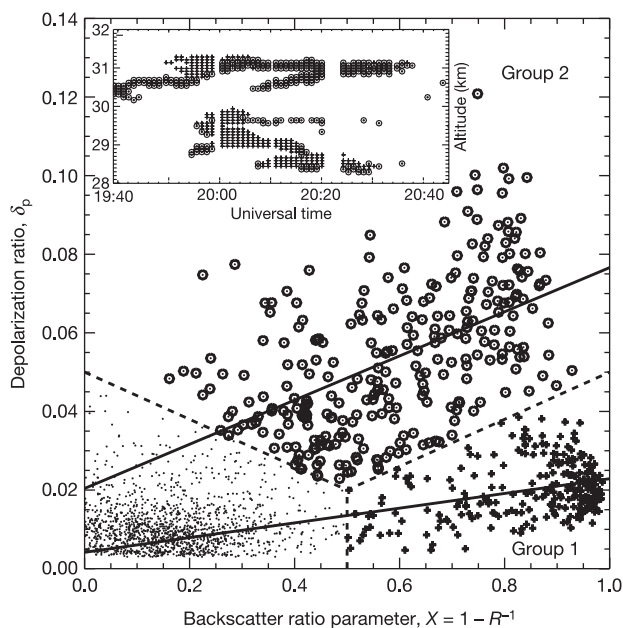


**Figure 4 | Evidence that the lidar backscatter was due to non-spherical particles.** Plotted is the lidar-derived depolarization ratio  $\delta_p = S_p/S_s$  as a function of total backscatter parameter  $X = 1 - R^{-1}$ . Here  $S_p$  and  $S_s$  are the perpendicular and parallel polarized signal components, respectively, and  $R$  is the backscatter ratio. Divisions (dashed lines) have been assigned on the basis of the apparent clustering of points into distinct groups with the weighted linear regression fits to the rightmost (Group 1, crosses) and upper (Group 2; dotted circles) associations also shown (solid lines). The inset shows where points from Groups 1 and 2 lie in relation to the cloud. Clustered in the lower left-hand quadrant of the main plot are points representing the background aerosols that do not show a preferred association with the cloud features. Photon-counting noise, as well as gravity waves unresolved by the AIRS data, tends to scatter the points in the  $X$ -axis. For the non-spherical (solid) aerosols, Group 1 are characterized by low depolarization and high backscatter ratios and are associated with the leading edges of the strongest cloud layers. They have a limiting depolarization ratio  $\delta_1$  ( $\lim_{X \rightarrow 1} \delta_p$ ) of  $2.3 \pm 0.4\%$ . Group 2 particles have a wide range of depolarization and backscatter ratios, with  $\delta_1 = 7.6 \pm 0.7\%$ . The backscatter coefficient for Group 1 was mean  $\beta_a = (2.351 \pm 0.003) \times 10^{-7} \text{ m}^{-1} \text{ sr}^{-1}$  and total  $\beta_a = (5.831 \pm 0.008) \times 10^{-5} \text{ m}^{-1} \text{ sr}^{-1}$ , and for Group 2 mean  $\beta_a = (4.31 \pm 0.01) \times 10^{-8} \text{ m}^{-1} \text{ sr}^{-1}$  and total  $\beta_a = (1.197 \pm 0.004) \times 10^{-5} \text{ m}^{-1} \text{ sr}^{-1}$ . The Group 1 aerosols produced similar depolarization to those associated with an anomalous aerosol layer observed by lidar in the Arctic winter of 2000–2001 (ref. 27). This similarity strengthens the case for a meteoric origin for the Arctic layer.

1. Ceplecha, Z. et al. Meteor phenomena and bodies. *Space Sci. Rev.* **84**, 327–471 (1998).
2. Hunten, D. M., Turco, R. P. & Toon, O. B. Smoke and dust particles of meteoric origin in the mesosphere and stratosphere. *J. Atmos. Sci.* **37**, 1342–1357 (1980).
3. Jenniskens, P. Meteor induced chemistry, ablation products, and dust in the middle and upper atmosphere from optical spectroscopy of meteors. *Adv. Space Res.* **33**, 1444–1454 (2004).
4. Artemieva, N. A. & Shuvalov, V. V. Motion of a fragmented meteoroid through the planetary atmosphere. *J. Geophys. Res.* **106**, 3297–3309 (2001).
5. Ceplecha, Z., Spurny, P., Borovicka, J. & Kecklikova, J. Atmospheric fragmentation of meteoroids. *Astron. Astrophys.* **279**, 615–626 (1993).
6. ReVelle, D. O. in *Proc. Asteroids, Comets, Meteors (ACM 2002, International Conference, 29 July–2 August 2002, Berlin, Germany)* (ed. Warmbein, B.) ESA SP-500, 127–136 (ESA Publications, Noordwijk, Netherlands, 2002).
7. Brown, P., Spalding, R. E., ReVelle, D. O., Tagliaferri, E. & Worden, S. P. The flux of small near-Earth objects colliding with the Earth. *Nature* **420**, 294–296 (2002).
8. Edwards, W. N., Brown, P. & ReVelle, D. O. Bolide Energy Estimates from Infrasonic Measurements. *Earth, Moon and Planets* (Kluwer Academic, Dordrecht, in the press).
9. Britt, D. T. & Consolmagno, G. J. Stony meteorite porosities and densities: A review of the data through 2001. *Meteorit. Planet. Sci.* **38**, 1161–1180 (2003).
10. Klekociuk, A. R., Lambert, M. M., Vincent, R. A. & Dowdy, A. J. First year of Rayleigh lidar measurements of middle atmosphere temperatures above Davis, Antarctica. *Adv. Space Res.* **32**, 771–776 (2003).
11. Santacesaria, V., Mackenzie, A. R. & Stefanutti, L. A climatological study of polar stratospheric clouds (1989–1997) from LIDAR measurements over Dumont d'Urville (Antarctica). *Tellus B* **53**, 306–321 (2001).
12. Gobbi, G. P., Di Donfrancesco, G. & Adriani, A. Physical properties of stratospheric clouds during the Antarctic winter of 1995. *J. Geophys. Res.* **103**, 10859–10873 (1998).
13. Fetzer, E. et al. AIRS/AMSU/HSB Validation. *IEEE Trans. Geosci. Remote Sens.* **41**, 418–431 (2003).

14. Morris, G. A., Ziemke, J., Gleason, J. & Schoeberl, M. R. Trajectory mapping: A tool for satellite data validation. *J. Geophys. Res.* **105**, 17875–17894 (2000).
15. Swinbank, R. & O'Neill, A. A. Stratosphere-troposphere data assimilation system. *Mon. Weath. Rev.* **122**, 686–702 (1994).
16. Adachi, H., Shibata, T., Iwasaka, Y. & Fujiwara, M. Calibration method for the lidar-observed stratospheric depolarization ratio in the presence of liquid aerosol particles. *Appl. Opt.* **36**, 6578–6595 (2001).
17. Mishchenko, M. & Travis, L. D. Capabilities and limitations of current FORTRAN implementation of the T-Matrix method for randomly oriented, rotationally symmetric scatterers. *J. Quant. Spectrosc. Radiat. Transf.* **60**, 309–324 (1998).
18. Mishchenko, M. & Hovienier, J. W. Depolarization of light backscattered by randomly oriented nonspherical particles. *Opt. Lett.* **20**, 1356–1358 (1995).
19. Jager, C. *et al.* A database of optical constants of cosmic dust analogs. *J. Quant. Spectrosc. Radiat. Transf.* **79/80**, 765–774 (2003).
20. Rothman, L. S. *et al.* The HITRAN molecular database: Editions of 1991 and 1992. *J. Quant. Spectrosc. Radiat. Transf.* **48**, 469–507 (1992).
21. Lazzarin, M., di Martino, M., Barucci, M. A., Doressoundriam, A. & Florczak, M. Compositional properties of Near-Earth Asteroids: spectroscopic comparison with ordinary chondrite meteorites. *Astron. Astrophys.* **327**, 388–391 (1997).
22. Penner, J. E. *et al.* in *Climate Change 2001: The Scientific Basis. Contribution of Working Group I to the Third Assessment Report of the Intergovernmental Panel on Climate Change* (ed. Houghton, J. T. *et al.*) 289–348 (Cambridge Univ. Press, Cambridge, 2001).
23. Toon, O. B. & Farlow, N. H. Particles above the tropopause: Measurements and models of stratospheric aerosols, meteoric debris, nacreous clouds, and noctilucent clouds. *Annu. Rev. Earth Planet. Sci.* **9**, 19–58 (1981).
24. Lal, D. & Jull, A. J. T. Atmospheric cosmic dust fluxes in the range  $10^{-4}$  to 10 centimeters. *Astrophys. J.* **576**, 1090–1097 (2002).
25. Karner, D. B. *et al.* Extraterrestrial accretion from the GISP2 ice core. *Geochem. Cosmochim. Acta* **67**, 751–763 (2003).
26. Fisher, A. A., Hawkes, R. L., Murray, I., Campbell, M. D. & LeBlanc, A. G. Are meteoroids really dustballs? *Planet. Space. Sci.* **48**, 911–920 (2000).
27. Gerding, M. *et al.* Observation of an unusual mid-stratospheric aerosol layer in the Arctic: possible sources and implications for polar vortex dynamics. *Ann. Geophys.* **21**, 1057–1069 (2003).

**Supplementary Information** is linked to the online version of the paper at [www.nature.com/nature](http://www.nature.com/nature).

**Acknowledgements** The Davis lidar observations are funded by the Department of the Environment and Heritage of the Australian Government. We thank D. McCormack and R. L. Hawkes for discussions. This work was supported in part by the Canada Research Chair programme, the Natural Sciences and Engineering Research Council of Canada and The Aerospace Corporation's Independent Research and Development programme.

**Author Contributions** A.R.K. developed the Davis lidar instrument, identified and analysed the bolide event in the lidar observations and co-wrote this Letter. P.G.B. helped interpret global infrasound network data, performed entry modelling and co-wrote this Letter. W.N.E. analysed global infrasound network data. D.O.R. performed entry modelling and helped interpret the global infrasound network. D.W.P., R.E.S., E.T. and B.B.Y. analysed Department of Defense and Department of Energy satellite data. J.Z. undertook initial and follow-up lidar observations, and assisted with data analysis.

**Author Information** Reprints and permissions information is available at [npg.nature.com/reprintsandpermissions](http://npg.nature.com/reprintsandpermissions). The authors declare no competing financial interests. Correspondence and requests for materials should be addressed to A.R.K. ([andrew.klekociuk@aad.gov.au](mailto:andrew.klekociuk@aad.gov.au)).